Etching-enhanced ablation and the formation of a microstructure in silicon by laser irradiation in an SF_6 atmosphere

S. Jesse, A.J. Pedraza,[a] and J.D. Fowlkes
Department of Materials Science and Engineering, The University of Tennessee, Knoxville, Tennessee 37996-2200

J.D. Budai
Solid State Division, Oak Ridge National Laboratory, Oak Ridge, Tennessee 37831-6056

(Received 25 April 2001; accepted 5 February 2002)

Sequential pulsed-laser irradiation of silicon in SF_6 atmospheres induced the formation of an ensemble of microholes and microcones. Profilometry measurements and direct imaging with an intensifying charge-coupled device camera were used to study the evolution of this microstructure and the laser-generated plume. Both the partial pressure of SF_6 and the total pressure of an SF_6-inert gas mixture strongly influenced the maximum height that the microcones attained over the initial surface. The cones first grew continuously with the number of pulses, reached a maximum, and then began to recede as the number of laser pulses increased further. The growth of the cones was closely connected with the evolution of the laser-generated plume.

I. INTRODUCTION

Mechanical spallation, expulsion of small droplets from a transiently laser-melted layer, desorption of atoms and ions, and evaporation have been identified as some of the processes responsible for laser-induced ablation.[1] When a reactive atmosphere is present, ablation can be enhanced if volatile compounds within the target material are produced and/or if the reaction yields a surface layer that is easier to remove by laser irradiation than the target material itself. In this paper this process is identified as etching-enhanced laser ablation. Generally, part of the material removed from the target can be collected on a substrate and this constitutes the basic step for the deposition of thin films by pulsed laser ablation. In this process, laser irradiation can produce very drastic changes in the topography of the target. Commonly, these changes strongly decrease the deposition rate. When silicon is irradiated in air, or more generally in O_2-rich atmospheres, with 1000 laser pulses at a power of 130 MW/cm^2, a dense array of high aspect ratio columns forms on the surface. These columns are 20 to 70 μm high and 2–3 μm in diameter.[2–10] An array of conical microstructures is produced when laser irradiation is performed under an SF_6 atmosphere.[11–13]

Formation of conelike structures due to pulsed-laser irradiation is well documented for a wide range of materials.[14] In many instances preferential etching could explain the formation of these structures.[14] In the case of the formation of cones under sulfur hexafluoride (SF_6) atmospheres in silicon this explanation is not sufficient because the cones protrude above the initial surface.[11,12] Moreover, we have studied laser-induced silicon microstructuring and have observed that it strongly depends on the irradiation atmosphere.[2–5,12] By contrast, under the same irradiation conditions of wavelength, pulse fluence, and accumulated fluence, no columns are formed if the irradiation is performed under 1 atm of high-purity nitrogen or argon.[2,5]

We have proposed a mechanism to explain this relief in SF_6 as well as the morphological details of the microstructure shown in Fig. 1. This mechanism involves the ablation of silicon from regions surrounding the emerging features and the enhanced redeposition of silicon on top of them.[5,11,12] It was proposed that the deep grooves and pits between cones result from a laser-induced ablation phenomenon and that this receding part of the surface surrounding each of the cones is the source of an intense flux of silicon-rich vapor. Growth was explained to occur through a synergism: the pulsed-laser *melting* of the cone tips and *deposition* of silicon from the vapor produced by pulsed-laser *ablation/etching.* The reason for the tips of the cones being strongly preferred sites for deposition is that they are melted; thence a very high axial growth rate could ensue. We have inferred the growth process just outlined from experimental studies reported in a series of papers and pointed out that it is based on the theory of film deposition.[15] Similar

[a]e-mail: apedraza@utk.edu

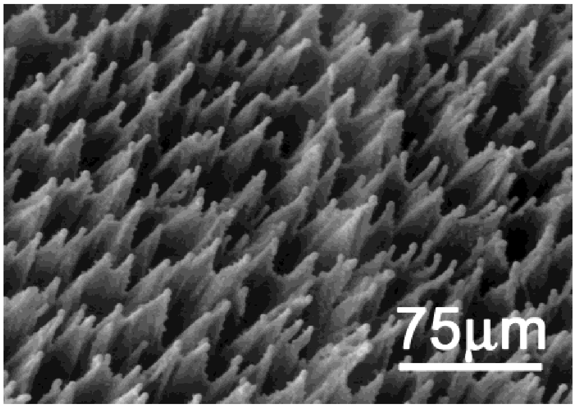

FIG. 1. Micrograph of a typical (100) Si microstructure obtained after 1500 laser pulses at a fluence of 1.5 J/cm^2.

concepts have been used to explain the mechanism of growth of silicon whiskers by the vapor–liquid–solid method (VLS).[16,17] In the present case we proposed that the pulsed-laser irradiation has two, almost simultaneous, effects: it provides the flux of silicon-containing molecules and it melts the tips of the cones. At variance with VLS, the laser process does not require the presence of a catalyst.[5]

During laser irradiation, there are liquid, solid, and vapor phases involved, and they interact in a very complex manner. Sanchez *et al.* proposed that a hydrodynamic instability was responsible for the growth of columns in Si irradiated in air.[8–10] We examined the possibility of this process using our experimental results for oxygen-rich atmospheres and concluded that it was unlikely that straight columns would grow by this mechanism.[2]

This paper is part of a system of studies that focused on the effects of SF_6-rich atmospheres on the production of a surface microstructure in silicon. In this case, it was not very difficult to separate the liquid effects from the ablation products effects by simply switching atmospheres from SF_6 to He, as previously reported.[12] Using scanning electron microscopy (SEM), we have followed the evolution of a set of identified cones in well developed microhole/microcone structures grown under SF_6 and observed that switching to inert Ar gas caused the cone growth to stop. When irradiation was subsequently resumed in the SF_6 atmosphere, the growth of microcones resumed. If the motion of liquid would be responsible for growth of the cones, growth should not be stopped as we change atmospheres, contrary to what was observed. It is well recorded in the literature that SF_6 etches silicon during irradiation.[18] Indeed, we always observed the formation of microholes preceding the formation of microcones during irradiation of SF_6. No effects of this sort are observed when the irradiation is done in Ar under similar conditions of energy and gas pressure. It was concluded that the profuse ablation of etching products under SF_6 was responsible for cone growth. A variety of other reported experiments and very simple calculations convinced us that the ablation products, which include small clusters and particles, are responsible for cone growth.[5,11,12] The microstructuring initial stages, however, can be traced to surface perturbations of the laser-induced melt that are generated in the liquid, but cone growth begins only once microholes exist. A very detailed study of these initial stages and their aftermath together with a calculation that predicts their spacing is presented in another paper.[19]

In this paper we report on the topographical evolution as a function of the number of laser pulses at various pressures. *In situ* studies help to establish a relationship between the evolution of the fluorescent plume and the growth and dissolution of cones, which are accompanied by the deepening of microholes. Our focus here is to study the interrelationship between the formation of microholes, the growth of microcones and the evolution of the plume with the aim of firmly establishing the overall growth mechanisms. Studies of the plume evolution during laser irradiation at high background gas pressure are presented for the first time. At difference with other studies of the plume, under these high pressures the plume is confined to microscopic distances from the target and a long focal microscope is required to image it.

II. EXPERIMENTAL TECHNIQUES

Silicon substrates were irradiated using a Lambda Physik LPX-305i (Göttingen, Germany) excimer laser operating at 248-nm wavelength with a pulse duration of 25 ns. All laser treatments were carried out at nearly normal laser incidence. The laser beam emerging from the laser cavity was directed to an optic bench using a MgF_2-coated fused silica mirror.

The optic bench contained an aperture, a fused-silica lens array, and the irradiation chamber. The aperture, 1 cm × 2.5 cm, partly removed the low-energy tails of the trapezoidal laser beam. The laser fluence was varied by adjusting the position of the fused-silica lens array with respect to the sample holder in the irradiation chamber.

Test grade *p*-type, boron doped silicon wafers of (100) and (111) orientations were used in the experiments. The specified thickness range of the wafers was 475–525 μm, and the resistivity ranges were 1.0–6.2 and 1–100 Ω cm for the (100) and (111) wafers, respectively. The native oxide present on each polished substrate was not removed prior to laser irradiation. The difference in crystalline orientation did not translate into any significant difference in the growth of cones.

The laser treatments were carried out in two different background gases: inert He and reactive SF_6, both 99.95% pure. The irradiation chamber was pumped to a base pressure of 10^{-7} torr and then filled with the gas of choice. *In situ* imaging of the ablation process was performed using a Questar QM100 (Montpelier, MD) long focal distance microscope attached to a Princeton Instruments PI-MAX (Tucson, AZ) intensifying charge-coupled device (ICCD) camera. The focal distance of the microscope was set to approximately 24 cm. All lenses within the microscope are fused silica and transparent to the 248-nm laser radiation. This arrangement is required because most of the light coming from the plume is in the UV range. The charge-coupled device is comprised of a 512 × 512 imaging array, and the minimum acquisition time (pulse width) for the camera is 2 ns. The maximum resolution achieved using this setup was approximately 1 μm/pixel.

III. PROFILOMETRY STUDIES

All of the profilometry measurements were done on laser-microstructured (100) silicon substrates. The vertical resolution of the profilometer is better than 10 nm, but the lateral resolution is much poorer because the tip diameter is 5 μm. Figure 2 shows the profiles of the grooves on the surface of two silicon specimens after irradiation with 200 pulses at a fluence of 2.9 J/cm^2 in two different atmospheres, He and SF_6. It can be seen that no columns or cones have yet evolved. The grooves produced under He are very shallow indicating that very little ablation took place [Fig. 2(a)]. By contrast, 0.25-μm-deep trenches were produced under an atmosphere of SF_6 [Fig. 2(b)], showing that more material was removed during the irradiation in this atmosphere. As previously analyzed, the etching is most probably made possible by the decomposition of SF_6 during laser irradiation.[11,12] The fluorine produced by the decomposition is absorbed in the near-surface region of the specimen where it reacts with Si producing a volatile compound. At temperatures higher than 800 K the etching product with the highest concentration is SiF_2.[18] Thus, the laser irradiation causes decomposition of SF_6, heats the surface of the silicon, and promotes desorption of the volatile products generated in the near surface region of the target. This set of phenomena provides the signature of an etching-enhanced ablation process: the irradiation-induced formation of a compound that is easily ablated by irradiation as well.

Profilometry measurements were used to follow the growth of the cones (Fig. 3). These measurements were performed on specimens irradiated at 2.5 J/cm^2 under a total background pressure of 0.5 bar of SF_6. No cone growth above the initial surface was detected with 500 pulses [Fig. 3(a)], but with 750 pulses the average

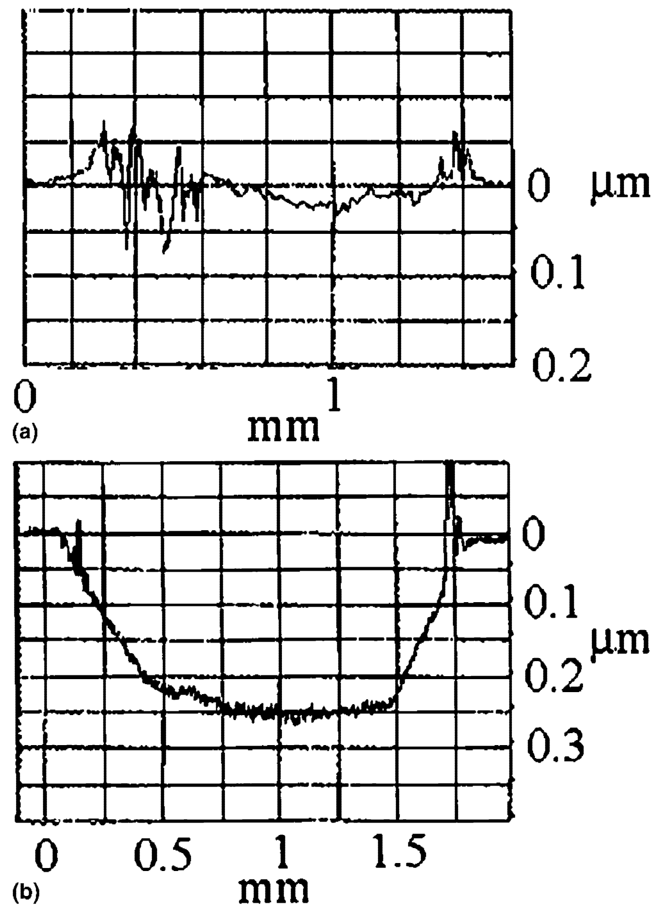

FIG. 2. Profiles of a Si substrate irradiated with 200 consecutive pulses at a laser fluence of 2.9 J/cm^2, in 1 bar of (a) He and (b) SF_6.

cone in the central region of the laser spot grew to a height of 10 μm [Fig. 3(b)]. The average height of the cones increased steadily with the number of pulses reaching a maximum of approximately 40 μm after 1000 pulses [Fig. 3(c)]. Thence, there was a steady decrease in height as the number of laser pulses was further increased [Figs. 3(d)–3(h)]. After 2250 pulses the average height decreased to 10 μm [Fig. 3(h)].

Similar results were obtained by varying the pressure of SF_6 between 0.125 and 1 bar. The maximum height was reached after 1000 to 1500 pulses and a significant decrease in cone height was observed after 2250 pulses. As the background pressures of SF_6 were increased between 0.125 and 0.5 bar, irradiation produced an increase in the cones' height. On the other hand, when the pressure was increased between 0.5 and 1 bar the cones' height decreased. Figures 4(a)–4(h) show height profiles as a function of pressure after 2000 pulses at a laser fluence of 2.5 J/cm^2. The serrated pattern is a clear indication of the presence of microcones. The microcones grew in every instance around microholes as shown in the SEM micrograph of Fig. 5.

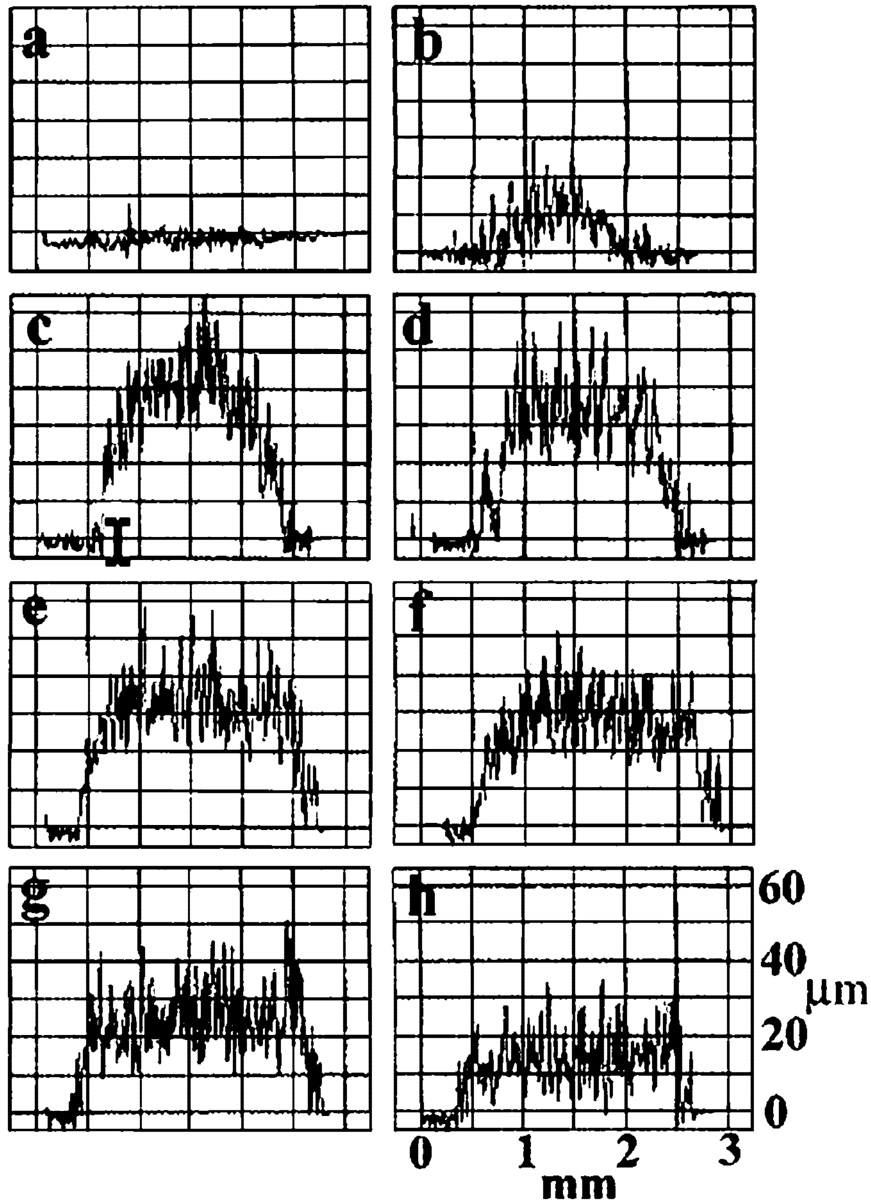

FIG. 3. Profiles of a Si substrate irradiated at a laser fluence of 2.5 J/cm^2 under 0.5 bar of SF_6 at an increasing number of pulses: (a) 500; (b) 750; (c) 1000; (d) 1250; (e) 1500; (f) 1750; (g) 2000; (h) 2250.

To better understand the effect of ambient atmosphere on redeposition, irradiations were performed using different proportions of SF_6 and Ar while maintaining the total background gas pressure at a constant value of 1 bar. The cones' height increased and then decreased with an increase in the partial pressure of SF_6 [Figs. 6(a)–6(d)]. The maximum height was attained at a partial pressure of 0.5 bar of SF_6 [Fig. 6(c)]. This was similar to the dependence detected when a background gas of SF_6 alone was used. However, the maximum height of the cones in this case was greater than when the specimens were irradiated under a gas mixture with a partial pressure of 0.5 bar of SF_6.

IV. EVOLUTION OF THE LASER GENERATED PLUME AND ITS RELATION WITH THE SURFACE MICROSTRUCTURE

The evolution of a cone structure on a (111) silicon target over multiple pulses of laser irradiation was followed using the ICCD-microscope setup. The irradiations were performed at a fluence of 3.1 J/cm^2 and at various background pressures of SF_6 ranging from 0.1 to 0.9 bar. Figure 7 illustrates the relative orientation of target, microscope image plane, and incident beam. All the images were taken nearly edge-on; that is, the irradiated surface was at an angle of approximately 5°

with the normal to the image plane of the microscope. In this way the line of cones at the edge of the substrate could be clearly observed without significant interference from the cones formed beyond the target edge. The surface was fully irradiated up to the edge as the center of the laser spot was positioned at the edge of the target. The edge of the sample was undercut to eliminate reflection of the incident beam into the camera setup and also

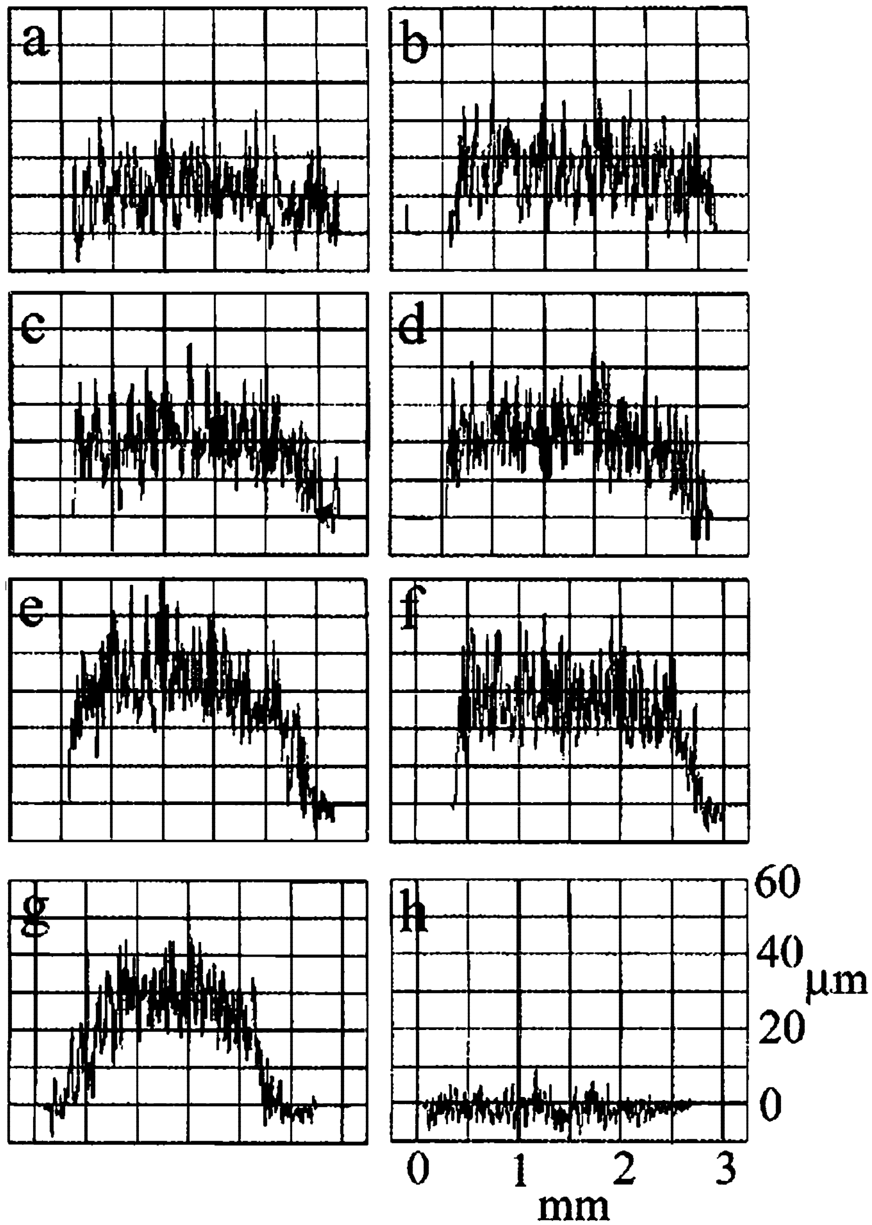

FIG. 4. Profiles of different Si substrates irradiated at a laser fluence of 2.5 J/cm^2 with 2000 sequential pulses, under SF_6 pressures of the following: (a) 1.0; (b) 0.875; (c) 0.75; (d) 0.625; (e) 0.5; (f) 0.375; (g) 0.25; (h) 0.125 bar.

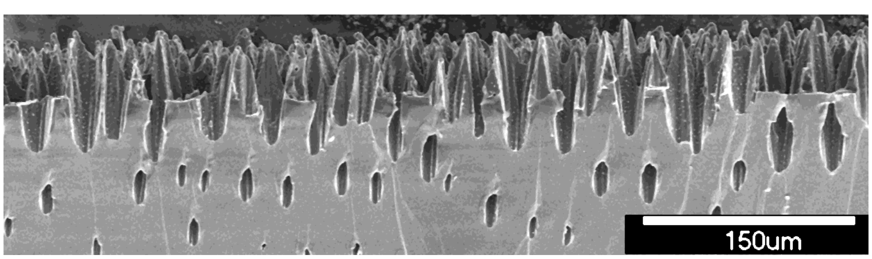

FIG. 5. Cross-section SEM of a Si substrate irradiated at a laser fluence of 2.5 J/cm^2 after 2000 pulses under 0.5 bar of SF_6.

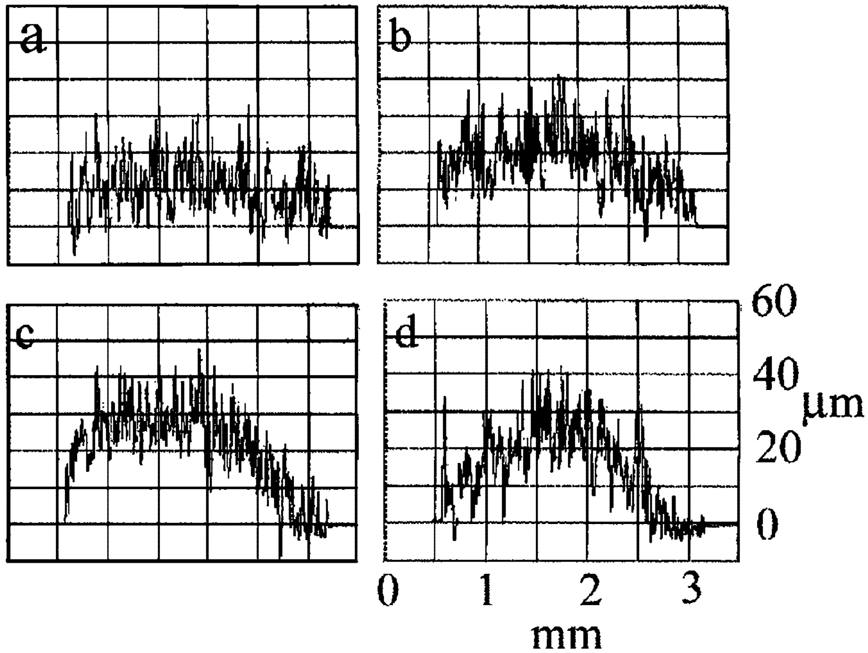

FIG. 6. Profiles of different Si substrates irradiated at a laser fluence of 2.5 J/cm^2 with 2000 pulses at a total pressure of 1 bar of SF_6 and Ar mixtures. The partial pressure of SF_6 is the following: (a) 1.0; (b) 0.75; (c) 0.50; (d) 0.25 bar.

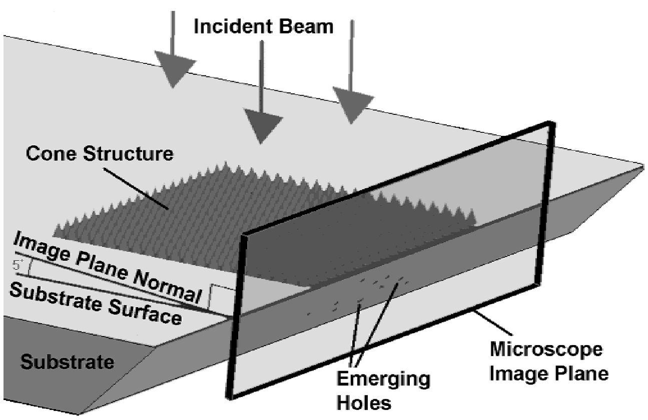

FIG. 7. Schematic drawing illustrating the relative orientation of target, microscope image plane, and incident beam.

make possible the detection of microholes formed near the edge during the ablation process. In the schematic drawing they are represented by small dots on the undercut surface.

The nominal time that the ICCD gate is open is defined as the pulse width and is equal to the time taken to acquire one image. The time elapsed between the initial arrival of the laser beam to the target and the acquisition of the image is defined as the delay time. One methodology of image acquisition was to maintain a constant delay time for each image. This acquisition mode is referred as "continuous" mode, and it is used primarily to characterize changes associated with the number of laser pulses. Using this acquisition mode, no plume was detected until the sample was irradiated with approximately 500 laser pulses. This result is congruent with profilometry measurements that reveal a relatively smooth surface and an ablation rate of only 1.2 nm/pulse up to 400 pulses.

The ICCD camera first detects microcones and microholes, together with the formation of a plume at 550 pulses. The development of cones and the evolution of the plume were followed at a constant delay time of 55 ns and a pulse width of 4.5 ns for a total of 22,000 pulses. After 55 ns of delay time the laser light, which has a FWHM of 25 ns, has essentially ceased, but the substrate continues to be immersed in a fluorescent plume. Figures 8(a)–8(h) show selected images taken respectively after 520, 550, 600, 700, 800, 900, 1300, 1700, and 22,000 pulses. The imaged plume extends across the entire width of the exposed area. The leading edge of the plume is clearly delineated in these images. This light is due only to the plume components that decay from excited electronic states emitting visible and UV photons. Nonemitting atoms, ions, molecules, or clusters are not detected.[20] The tip of the emerging cones in Fig. 8(b)–8(d) can be seen as small bright spots elevated above the surface of the substrate. In these first images the edge of the fluorescent plume extends up to 40 to 60 μm beyond the tips of the cones, and it is higher in the region where cones show fastest growth.

In the early stages of growth we observed that the plume height is not the same throughout the irradiated area. It is higher in the regions where the cones are growing faster. When the cones reach a certain height the plume tends to become higher in another area, and cones

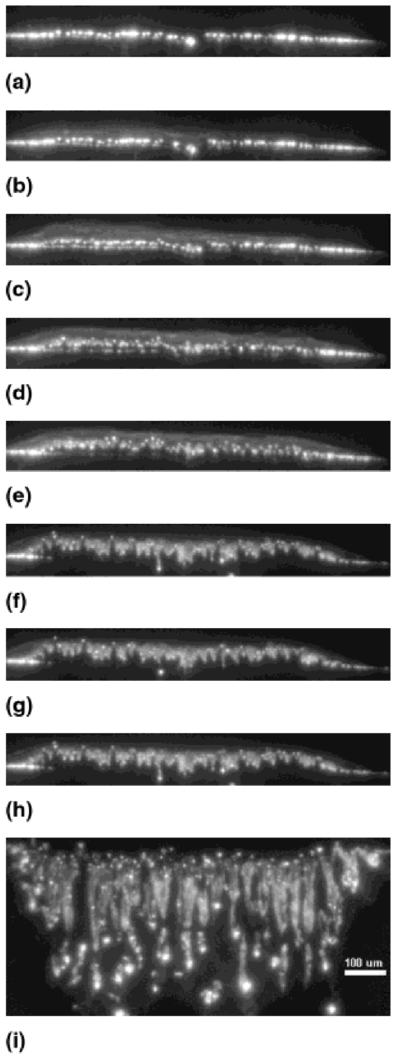

FIG. 8. Evolution of microcones and microholes in Si irradiated at 3.1 J/cm^2 in SF_6 at a pressure of 0.5 bar. ICCD images were taken in continuous mode with a delay time of 55 ns. Parts (a) through (h) show the microstructure and the plume at 520, 550, 600, 700, 800, 900, 1300, 1700, and 22,000 sequential pulses, respectively.

start to develop further in this area. After 900 pulses [Fig. 8(e)] the cone profiles are well resolved by the long focal distance microscope. Together with the growing microcones, deepening microholes are observed in Figs. 8(e)–8(i) as bright spots below the initial surface, and when holes perforate the lateral surface, the bright spots at the bottom of the holes reveal a strong increase in fluorescence [Figs. 8(f)–8(i)]. The maximum ablation rate in the holes measured by the ICCD images was 1.4 μm/pulse, a value much larger than the 1.2 nm/pulse measured on flat surfaces. This measurement was performed by following the progression of a hole through the substrate during 20 sequential pulses. The advance of the hole is followed from the point in its wall that first emerges until the opposite side in its wall emerges, and thus, not further advance is detected. It is important to note that the ablation rate is not constant throughout the growth of the microhole. In the initial stages of formation of the hole, the ablation rate is comparatively small. As the depth increases, the number of internal reflections increases focusing more light to the bottom of the microhole. This in turn increases the ablation rate. As the hole deepens even further, light is dispersed more evenly on the walls of the microhole, maximum intensity drops, and as a consequence ablation slows. This can also be clearly realized by comparing the sequence of ICCD images shown in Fig. 8. In Fig. 8(f) two distinctive holes emerge in the center of the image that were not seen 400 laser pulses earlier, Fig. 8(e). For these, the average growth rate through the 400 laser pulses is approximately 200 nm/pulse. This result agrees very well with the ablation rate previously measured at the bottom of microholes using cross-sectional SEM images.[11] However, if the images of emerging holes in Fig. 8(h) are compared with those in Fig. 8(e), the hole mean deepening rate is now 20 nm/pulse. At this stage the cone structure is well under the initial surface.

Images of the target during irradiation can also be acquired by sequentially increasing the delay time from one exposure to the next. This mode is called sequential, and it is often used to characterize events during a single laser pulse. To study the evolution of the plume 20 to 40 images were acquired in sequential mode. Since the target is being modified with every pulse, it must be assumed that all the irradiation pulses produce identical results. This is a good approximation provided images are acquired over the span of few pulses. Because the modification of the target is appreciable only at intervals of hundreds of pulses, we can safely assume that very small changes take place at intervals of a few tens of pulses thus qualifying the results as representative of the changes within a single pulse. The plume evolution was studied by recording images in sequential mode between 800 and 900 pulses. Each image was captured 1 ns later than the preceding one. Figure 9 shows a set of images with delay times increasing from 45 to 90 ns showing the expansion of the plume under 0.5 bar of SF_6 and a laser fluence of 3 J/cm^2. The distance from the cone tips to the plume edge was measured using 30 images, and it was plotted as a function of the delay time (Fig. 10). We found that the drag model for describing the propagation of a laser-generated plasma fits the data well. This model predicts that the plume front should advance with time according to[20,21]

$$x = x_f(1 - e^{-\beta t}) \quad . \tag{1}$$

Fitting this equation to our data yielded the values $x_f = 46$ μm and $\beta = 47.5$ μs^{-1}.

In Fig. 11, the plume front propagation distance was plotted as a function of background pressure for various delay times. For a given delay time, the plume reaches a local maximum at 0.5 bar. The initial velocity as a function of pressure is plotted in Fig. 12. Although the maximum velocity was reached at 0.5 bar, remarkably the initial plume velocity increased again as the pressure was decreased below 0.2 bar. The profilometry measurements indicating a maximum cone height at either a partial or total pressure of 0.5 mbar of SF_6 correlate with the fact that both the plume front distance and the velocity also are at a maximum when the pressure is 0.5 bar.

V. X-RAY ANALYSIS

In strong contrast with the columns that grow when silicon is pulsed laser irradiated in air, cones grown under an SF_6 atmosphere are single crystals with the same orientation as the target. What is even more remarkable is that no significant line broadening has been detected in the x-ray analysis. Rocking curve analyses show that the original target had a line broadening of 0.0142° while

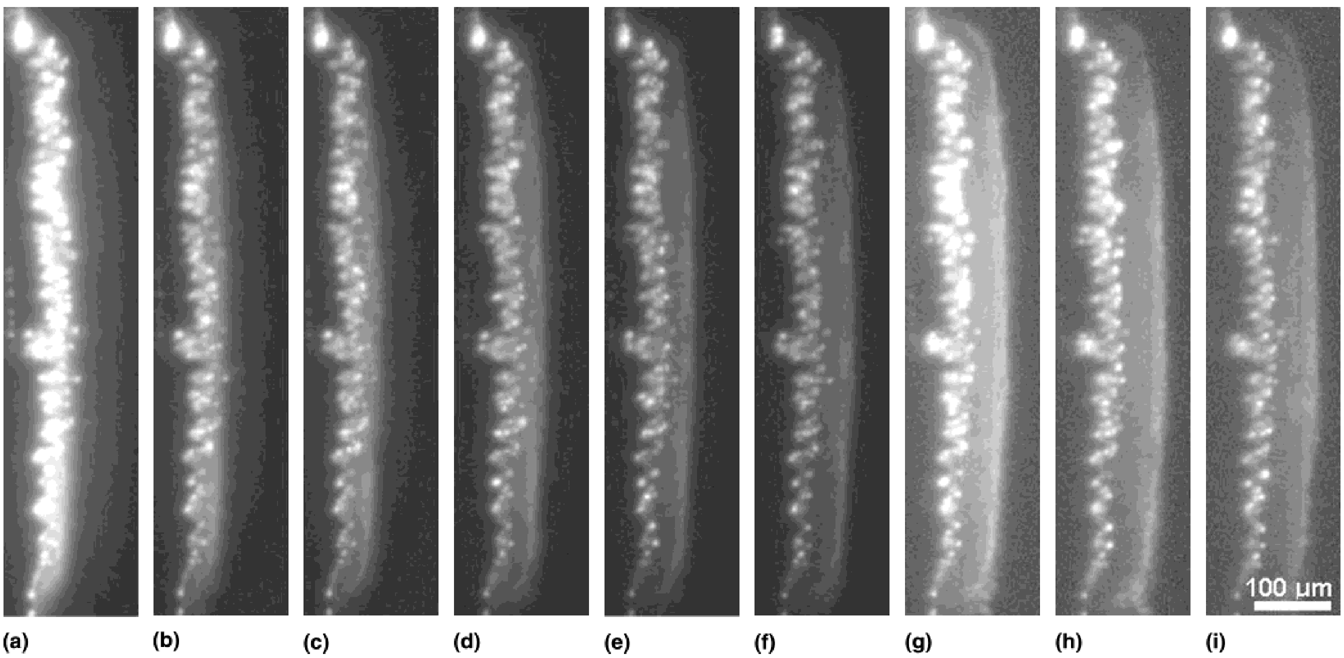

FIG. 9. Evolution of a laser-generated plume during ablation of Si at 3.1 J/cm^2 at a pressure of 0.5 bar of SF_6. Images were captured in sequential mode. Parts a through i correspond to delay times of 40, 50, 55, 60, 65, 70, 75, 80, and 95 ns.

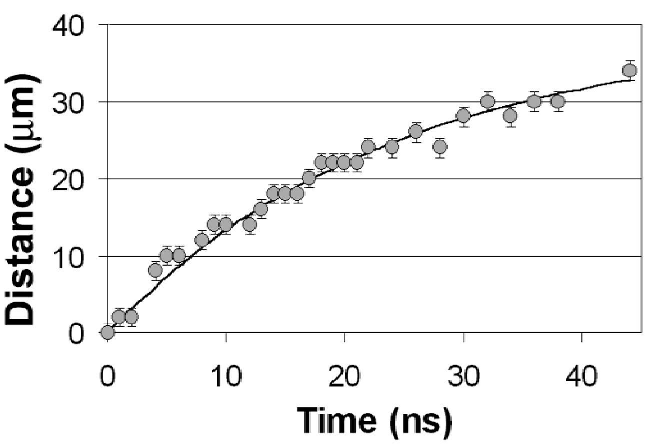

FIG. 10. Propagation distance of plume front edge from target surface as a function of time (0.5 bar SF_6, 3.1 J/cm^2, 800th–900th shot).

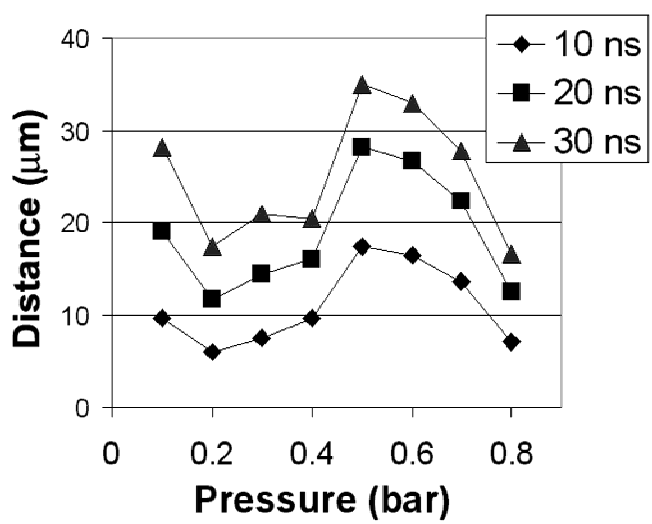

FIG. 11. Position of plume front edge relative to target surface as a function of background gas pressure for various delay times (3.1 J/cm^2).

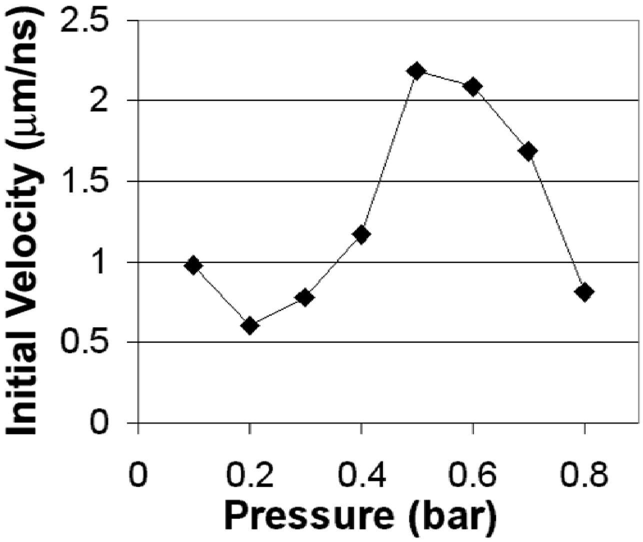

FIG. 12. Initial velocity of plume front as a function of SF_6 pressure, calculated using the drag model fit (3.1 J/cm^2).

the ablated target has a line broadening of 0.0179°. Both the lengthening and thickening of the cones are related to their ability to collect silicon from the silicon-rich vapor as well as small clusters that can form under the high-pressure background atmosphere.[11] Some of the volatile products that are being generated during the ablation process must be the constituents of the cones. Thus, we have proposed that the SiF_2 formed at the bottom of the holes and removed by the irradiation could react later at the tip and sides of the cones according to[18]

$$2SiF_2 \rightarrow SiF_4 + Si \quad .$$

This is a well-known reaction used in describing chemical vapor deposition of Si.[22] It can be expected that this decomposition will take place in the gas under the high supersaturation conditions prevalent during irradiation. The top and sides of the cones melted during irradiation are completely resolidified after 100–200 ns following irradiation. The solidification of silicon after nanosecond irradiation takes place by the advance of a solid/liquid interface moving from the nonmelted substrate.[23,24] If Si atoms and small clusters are incorporated while the sides and tips of the cones remain melted, resolidification should generate a single crystal with the same orientation as the substrate.

VI. SUMMARY AND DISCUSSION

The amount of silicon evaporated by laser irradiation in a He atmosphere at a fluence of 3 J/cm^2 is fairly small. The ablation rate of 1.2 nm/pulse in SF_6 on relatively flat surfaces is significantly larger than the laser-induced evaporation during irradiation in the noble gas atmosphere. We have named this process of ablation boosting etching-enhanced laser ablation. The maximum ablation rate in the microholes produced during multiple irradiation in SF_6 is of the order of 1.4 μm/pulse, 3 orders of magnitude higher than for a flat surface.

The profilometry results show that both the pressure and the nature of the gases present affect the microstructure produced during multiple pulsed-laser irradiation. Profilometry measurements also show that the cones' height attains a maximum when irradiation is conducted at a background pressure of 0.5 bar of SF_6. These results correlate with the *in situ* measurements of the maximum height of the plasma relative to the cone tips and the average velocity of the plasma as a function of SF_6 pressure. Both the plume front distance from the cone tips and the velocity are at a maximum when the SF_6 pressure is 0.5 bar. Although the maximum velocity was reached at 0.5 bar, the plume velocity increased again as the pressure was decrease below 0.2 bar (Fig. 12). These results suggest that SF_6 fulfills two roles: first, it acts as an etcher of silicon, and second, it exerts the background pressure that tends to restrict the expansion of the plume. An increase in the ambient background pressure produces an increase in etching rate thus increasing the pressure produced by the laser-generated plume. This increase in pressure is reflected in an increase in the velocity of the laser-generated plasma. However, as the background pressure is increased, the role of SF_6 as an etcher is increasingly counteracted by its role as a background gas that tends to slow the plume front. When a gas mixture of SF_6 and Ar at a constant total pressure of 1 bar is used, the maximum height of the cones is reached when the partial pressure of SF_6 is also 0.5 bar. However, the maximum height reached in this case is significantly lower than for the case where only 0.5 bar of SF_6 is present. This behavior is to be expected because the addition of Ar further contributes to contain the plasma without altering the etching power of the background gas.

The dynamics of growth and dissolution as a function of the number of laser pulses very clearly show a correlation between cone and plume evolutions. The cones grow continually until approximately 1200 pulses and at the same time the microholes continually deepen. Up to this point, the material ablated from within the microholes and redeposited at the tips of the cones is larger than the amount of silicon that is ablated from the cones' tips. Like any other laser-exposed area on the substrate surface, the cones were continually etched and ablated, but the plasma that surrounded them supplied the tip and sides with enough silicon to yield a net cone growth. The laser-melted silicon both at the cone's side and tip can efficiently collect both the silicon-rich vapor and small clusters that form at these relatively high ambient pressures. According to deposition theory a negligible supersaturation is required to initiate the deposition on the substrate.[15] The accommodation coefficient for molecules and atoms in a liquid is very close to one.[15] For this reason the deposition takes place preferentially at the cone tips which remain melted for a longer time than any other part of the cones.

As the holes deepen, the maximum plume height decreases as well. After approximately 1700 pulses, the fluorescent plume does not reach beyond the tips of the cones. If the fluorescent plume is an indication of the amount of ablated material present, less silicon-rich molecules or clusters are reaching the tips of the cones after 1700 shots. The balance between material ablated and material redeposited at the cone's tip becomes tilted toward the former and the cones begin to recede. At a sufficient number of pulses, the plume is concentrated at the bottom of the over 300-μm-deep holes, the silicon-rich plume is completely trapped, and the cones recede below the initial surface. The cones that once protruded 30 μm above the original surface after the first 1700 pulses are fully ablated after 22,000 pulses [Fig. 8(h)]. The bright spots at the bottom of the holes [Figs. 8(g)–8(i)] due to an enhanced fluorescence of the plume show that there is a correlation between the brightness of the plume and the amount of ablated material.

The sequence of Fig. 8 is fully consistent with the proposition that the cones, despite being constantly ablated by the laser, grow by the overwhelming influx of silicon-rich material transported from the microholes onto the molten tips. The evolution of the height profiles presented here as well as the joint development of microcones and microholes followed by SEM[11] are also consistent with the picture presented above.

To understand the causes of the extraordinarily large ablation in the microholes, the total intensity of laser radiation in a cavity was calculated taking into account the shape of the microhole, the absorption and reflections of the beam and the change in reflectivity with the angle of incidence. We assume that the incident light is not polarized. The shape of a typical microhole having a depth of approximately 140 μm was determined from cross-sectional SEM images, and it is outlined in Fig. 13(a) together with the path of some of the rays reflected inside the cavity. Because of the high reflectivity of a silicon surface to UV light and the steep slopes of the cavity walls that form an angle of approximately 5° with the incident beam, there is very strong concentration of laser energy at the bottom of the holes. Figure 13(b) shows the variation of intensity of the incident light along the surface of the hole. At the bottom of the microhole, this focusing effect produces a fourfold increase in the light intensity [Fig. 13(b)]. For a nominal laser fluence of 3 J/cm^2, this implies that the intensity at the bottom of the microholes shown in Figs. 8(d)–8(h) would be over 12 J/cm^2. Bright spots are seen at the bottom of the microholes in these figures. An intense absorption of laser light and a high rate of decomposition of SF_6 produced this hot plasma. The enhanced production of fluorine and possibly further ionization should result in a strong increase of the etching efficiency. Even in a vacuum background pressure, this very high laser intensity should produce a high ablation rate, as it is shown in the following.

The rate of evaporation of silicon can be approximately calculated by assuming that ablation takes place as the irradiated surface is rapidly heated resulting in a solid–gas interface progressing into the target material.[25] Melting is ignored as a part of the physical process that leads to ablation. This assumption is suitable since the

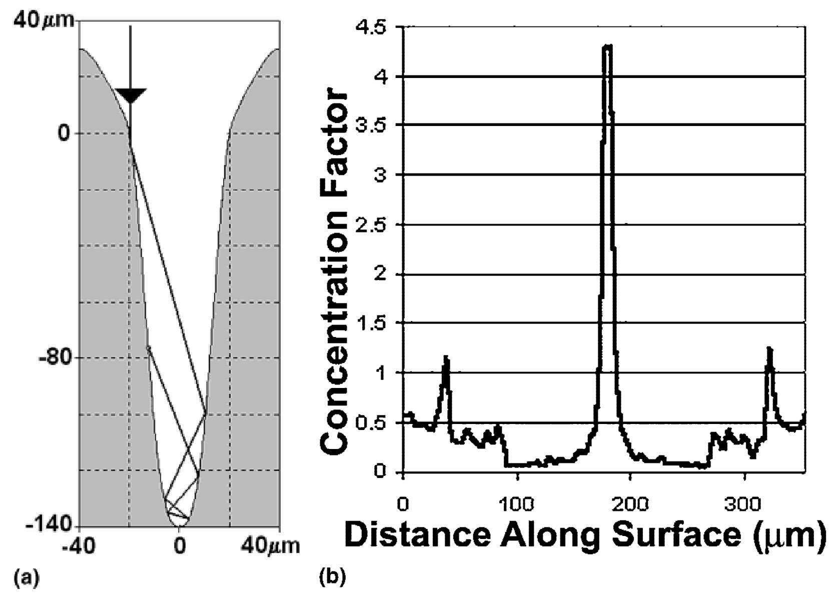

FIG. 13. (a) Profile of a typical microhole and path of a ray reflecting inside the cavity. (b) Ratio of local laser fluence to nominal fluence as a function of linear distance along microhole surface.

heat of vaporization is several times larger than the heat of melting and therefore dominates the energy balance. For silicon, the heat of melting is 50 kJ/mol while the heat of vaporization is 359 kJ/mol. Also, no atmosphere or plume–surface interactions are considered. In this model, the velocity and temperature of the solid–gas front is governed by the energy absorption and heat transfer characteristics of the target. The Drude–Zener theory of optical absorption is used which is based on a linear relation between absorptivity, A, and temperature, T_s. The following two relations can be obtained:[25]

$$AI = V_s \rho (L_v + c_p T_s) \quad , \tag{2}$$

$$V_s = V_0 \exp\left(\frac{-ML_v}{k_b T_s}\right) \quad , \tag{3}$$

where I is the laser fluence, ρ is the density of silicon, L_v is the latent heat of vaporization, c_p is the heat capacity, V_0 is the speed of sound in the material, M is the molar mass, and k_b is Boltzman's constant. The equations are then solved simultaneously to find V_s and T_s, the evaporation front velocity and temperature. At a laser fluence of 12 J/cm^2 (the estimated intensity at the bottom of the microholes), V_s is found to be 38.2 m/s. A rough estimate of the time required to establish steady state evaporation, t_c, is given by

$$t_c = \frac{\kappa}{V_s^2 c_p \rho} \quad , \tag{4}$$

where κ is the thermal conductivity. For the same high laser fluence, this equation yields $t_c = 5.8$ ns. If it is assumed that most of the evaporation takes place after the establishment of a steady-state front and until the end of the 25 ns pulse, this model gives an ablation rate of 0.6 μm/pulse for a laser fluence of 12 J/cm^2. This rate is 500 times higher than the ablation rate of a flat surface in the presence of SF_6.

The advance of the plume front as a function of time can only be measured with the ICCD camera is approximately the first 100 ns because the ambient gas quickly quenches the laser-induced fluorescent light. The pressure at which these measurements were performed was thousands of times higher than in other reported measurements of plume expansion.[20,21] At a pressure of 0.5 bar the plume front reaches 60 μm before the background gas quenches the excitations producing the fluorescent light. We have found that at these very early stages of plume expansion, the drag-force model fits better than the shock model originally described by Zel'dovich and Raizer.[26] In the drag-force model it is assumed that the ablation products are moving as a whole and that the background gas produces a viscous deceleration of the plume proportional to the expansion velocity,

$$\frac{d\upsilon}{dt} = -\beta\upsilon \quad . \tag{5}$$

This model leads to Eq. (1) and fitted values of maximum front distance $x_f = 46$ μm and drag coefficient $\beta = 47.5$ μs^{-1}.

Geohegan[20] observed a similar behavior for the ablation of $YBa_2Cu_3O_{7-x}$ in 100 mtorr of oxygen with a value of $x_f = 3.0$ cm and $\beta = 0.36$ μs^{-1}. The initial velocity of the plume

$$\upsilon_0 = \beta x_f \quad , \tag{6}$$

was in this case 1 cm/μs. The initial velocity of the plume due to ablation/etching of silicon in our case is 2.4 cm/μs indicating that the pressure of the gases produced during etching is very high. However our drag coefficient, β, is 150 times larger than in the case of ablation of $YBa_2Cu_3O_{7-x}$. This difference reflects the fact that the background gas pressure is almost 4000 times larger than in the $YBa_2Cu_3O_{7-x}$ experiments.

In summary, we have shown that the growth of the cones is closely correlated with the evolution of the laser-generated plume. This correlation is strong evidence that the silicon-rich material that is removed by an ablation-etching process from the microholes feeds the growth of the cones near them. The interplay between the deepening of microholes and growing of cones was revealed, showing a continuing evolution leading to a stage where holes are so deep that insufficient material reaches the cones to overcome the always ongoing ablation process. Then, for a sufficiently large number of pulses, the cones recede beneath the initial surface. It is shown that, at the bottom of the microholes, ablation is greatly enhanced due to multiple reflections and focusing of the laser beam.

ACKNOWLEDGMENTS

This research was sponsored by the National Science Foundation Grant No. DMR-9901238 and by the Oak Ridge National Laboratory, managed by UT-Battelle, LLC, for the U.S. Department of Energy under Contract DE-AC05-00OR22725.

REFERENCES

1. R. Kelly and A. Miotello, Mechanisms of Pulsed-Laser Sputtering, in *Pulsed Laser Deposition of Thin Films,* edited by D.B. Chrisey and G.K. Hubler (Wiley, New York, 1994), pp. 55–87.
2. A.J. Pedraza, J.D. Fowlkes, and D.H. Lowndes, Appl. Phys. Lett. **77,** 3018 (2000).
3. A.J. Pedraza, J.D. Fowlkes, and D.H. Lowndes, Appl. Phys. A **69,** S731 (1999).
4. D.H. Lowndes, J.D. Fowlkes, and A.J. Pedraza, Appl. Sur. Sci. **154,** 647 (2000).
5. A.J. Pedraza, D. Fowlkes, and D.H. Lowndes, Appl. Phys. Lett. **74,** 2322 (1999).
6. V.V. Voronov, S.I. Dolgaev, S.V. Lavrishchev, A.A. Lyalin, A.V. Simakin, and G.A. Shafeev, Phys. Vib. **7,** 131 (1999).

7. V.V. Voronov, S.I. Dolgaev, S.V. Lavrishchev, A.A. Lyalin, A.V. Simakin, and G.A. Shafeev, Quantum Electron. **30,** 710 (2000).
8. F. Sanchez, J.L. Morenza, and V. Trtik, Appl. Phys. Lett. **75,** 3302 (1999).
9. F. Sánchez, J.L. Morenza, R. Aguiar, J.C. Delgado, and M. Varela, Appl. Phys. Lett. **69,** 620 (1996).
10. F. Sánchez, J.L. Morenza, R. Aguiar, J.C. Delgado, and M. Varela, Appl. Phys. A **66,** 83 (1998).
11. J.D. Fowlkes, A.J. Pedraza, and D.H. Lowndes, Appl. Phys. Lett. **77,** 1629 (2000).
12. A.J. Pedraza, J.D. Fowlkes, S. Jesse, C. Mao, and D.H. Lowndes, Appl. Sur. Sci. **168,** 251–257 (2000).
13. T-H. Her, R.J. Finlay, C. Wu, S. Deliwala, and E. Mazur, Appl. Phys. Lett. **73,** 1673 (1998).
14. S.R. Foltyn, Mechanisms of Pulsed-Laser Sputtering, in *Pulsed Laser Deposition of Thim Films,* edited by D.B. Chrisey and G.K. Hubler (Wiley, New York, 1994), pp. 89–113.
15. J.P. Hirth and J.M. Pound, Prod. Mater. Sci. **11,** 107 (1963).
16. R.S. Wagner, in *Whisker Technology,* edited by A.P. Levitt (Wiley, New York, 1970), p. 47.
17. E.I. Givargizov, Curr. Top. Mater. Sci. **1,** 79 (1978).
18. D. Bauerle, *Laser Processing and Chemistry,* 2nd ed. (Springer, Berlin, Germany, 1996), p. 253.
19. A.J. Pedraza, S. Jesse, Y. Guan, and J.D. Fowlkes, J. Mater. Res. **16,** 3599 (2001).
20. D.B. Geohegan, Mechanisms of Pulsed-Laser Sputtering, in *Pulsed Laser Deposition of Thin Films,* edited by D.B. Chrisey and G.K. Hubler (Wiley, New York, 1994), pp. 115–165.
21. D.B. Geohegan, Appl. Phys. Lett. **60,** 2732 (1992).
22. G. Bloem and L.J. Giling, Curr. Top. Mater. Sci. **1,** 147 (1978).
23. S. De Unamuno and E. Fogarassy, Appl. Surf. Sci. **36,** 1 (1989).
24. R.F. Wood and G.E. Jellison, Jr., in *Semiconductors and Semimetals,* edited by R.F. Wood, C.W. White, and R.T. Young (Academic Press, Orlando, FL, 1984), Vol. 23, p. 165.
25. S.I. Anisimov, V.A. Khokhlov, *Instabilities in Laser-Matter Interaction* (CRC Press, Boca Raton, FL, 1995), p. 17.
26. Ya.B. Zel'dovich, and Yu.P. Raizer, in *Physics of Shocks Waves and High Temperature Hydrodynamics Phenomena* (Academic Press, New York, 1966), Vol. 1, p. 94.